Thermal Conductivity Measurements on Polycrystalline Silicon Microbridges Using the 3ω Technique

Patrick E. Hopkins[1]
Department of Mechanical and Aerospace Engineering,
University of Virginia,
P.O. Box 400746,
Charlottesville, VA 22904-4746

Leslie M. Phinney[2]
Engineering Sciences Center,
Sandia National Laboratories,
P.O. Box 5800,
Albuquerque, NM 87185-0346
e-mail: lmphinn@sandia.gov

The thermal performance of microelectromechanical systems devices is governed by the structure and composition of the constituent materials as well as the geometrical design. With the continued reduction in the characteristic sizes of these devices, experimental determination of the thermal properties becomes more difficult. In this study, the thermal conductivity of polycrystalline silicon (polysilicon) microbridges are measured with the transient 3ω technique and compared with measurements on the same structures using a steady state Joule heating technique. The microbridges with lengths from 200 μm to 500 μm were designed and fabricated using the Sandia National Laboratories SUMMiT V™ surface micromachining process. The advantages and disadvantages of the two experimental methods are examined for suspended microbridge geometries. The differences between the two measurements, which arise from the geometry of the test structures and electrical contacts, are explained by bond pad heating and thermal resistance effects. [DOI: 10.1115/1.3072907]

Keywords: thermal conductivity, 3ω technique, polycrystalline silicon, suspended microbridge, thermal boundary resistance

1 Introduction

The characteristic lengths of material features contained in microelectronic devices are continually decreasing while the power generation needs and requirements continue to increase [1]. This is creating a huge incentive for efficient and effective thermal management, especially for materials with characteristic lengths on the order of the mean free paths of the carriers. Reduction in these mean free paths results from fabrication processes that produce more carrier scattering mechanisms in the materials [2]. For example, consider fabricating a semiconductor microcantilever, which involves the deposition of several materials as well as lithographic etching. The types of materials used to create the structure influences several characteristics of the final microcantilever, including surface roughness, sizes of geometric and grain boundaries, lattice dislocations, and impurities, which increase phonon scattering events and can significantly alter the thermal properties of the final structure [3]. However, the contribution of these individual phonon scattering processes on the thermal properties of the structure is very difficult to predict without experimental characterization and thermal testing [3]. Therefore, accurate experimental testing of thermal properties in low dimensional structures is becoming increasingly important to effective thermal management in current and future microelectronic materials [4].

Electrically based measurements have been successful in measuring thermal properties in low dimensional silicon structures, which are common in microelectromechanical systems (MEMS) and integrated circuits. Steady state resistance methods have successfully measured the thermal conductivity of various silicon structures, including undoped [5] and doped [3] polycrystalline silicon (polysilicon) films, doped single crystalline free standing films [6] and microcantilevers [7], doped polysilicon suspended films [8–10], and doped polysilicon suspended microbridges [11–13]. The advantages of these steady state techniques are the ease of measurement and analysis. However, processing constraints and measurement methods that are not optimized to minimize error due to experimental factors (i.e., convection and radiation losses) and test structure geometries (i.e., electrical probe contact resistance and heat flow to underlying structures or substrates) can lead to a complicated analysis to determine the true conductivity of the structure. For example, Phinney et al. [11] used a steady state technique to measure the temperature dependent thermal conductivity of polysilicon microbridges attached to bulk bond/electrical contact pads. Although the room temperature thermal conductivity values agreed with those from the room temperature studied by Tai et al. [12,13], the temperature dependent values and trends did not agree with previously reported values of thermal conductivity of polysilicon [3,5,8–10]. These differences could be due to complications from contact resistance and heat transfer to the substrate. By using a transient measurement technique, such as the 3ω technique, these effects could be reduced in comparison to a steady state method.

The 3ω technique was originally used by Cahill [14,15] to measure the thermal conductivity of bulk dielectric solids across a wide range of temperatures from 30 K to 750 K. Since then, this technique has been extended to measure the thermal conductivity of dielectric thin films [16], periodic superlattice structures [17], and nonperiodic multilayered structures [18,19]. In addition, this technique was extended to platinum and carbon nanotube suspended micro- and nanobridges [20,21]. The 3ω technique has several characteristics that make it an attractive alternative for thermal conductivity measurements on a wide range of materials and structures. The periodic nature of 3ω can make measurements inherently insensitive to radiative and convective losses, depending on the test section geometry. Second, a properly chosen ω input and range can eliminate problematic boundary conditions

[1]Present address: Engineering Sciences Center, Sandia National Laboratories, P.O. Box 5800, Albuquerque, NM 87185-0346.

[2]Corresponding author.

Contributed by the Heat Transfer Division of ASME for publication in the JOURNAL OF HEAT TRANSFER. Manuscript received March 27, 2008; final manuscript received December 9, 2008; published online February 11, 2009. Review conducted by Robert D. Tzou. Paper presented at the 2008 International Conference on Micro/Nanoscale Heat Transfer (MNHT2008), Tainan, Taiwan, January 6–9, 2008.

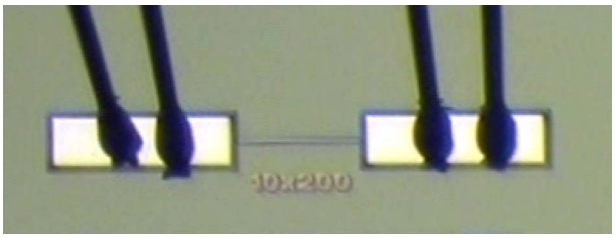

Fig. 1 Optical microscope image of a 10 μm wide×200 μm long test structure fabricated using the SUMMiT V™ process. The bond pads are 100 μm wide and 300 μm long. Two wires bonded to bond pad are visible in the image. The connections to the package are outside of the image.

that may exist between the sample and external test hardware [19]. Finally, since 3ω is a nondestructive technique, certain device geometries and material systems used in the high-powered microelectronic device systems of interest can be examined in their as-used conditions or with minimal post processing.

In this study, the thermal conductivity of polycrystalline silicon suspended bridge structures are measured with the 3ω technique. To the knowledge of the authors, this represents the first measurements of polysilicon bridges with the 3ω technique. The thermal conductivity of these same structures is also measured with a steady state resistance method, which allows for comparisons among the thermal conductivity measurement techniques. The suspended structures are fabricated using the Sandia Ultraplanar Multilevel MEMS Technology (SUMMiT V™) process [22,23]. In Sec. 2, the SUMMiT V™ process is described along with the test samples. The specific 3ω setup, analysis method, and assumptions are explained in Sec. 3. Section 4 presents the temperature dependent 3ω thermal conductivity results and compares them to the steady state measurements. The differences between the two measurements can be ascribed to contact and bond pad effects, for which steady state techniques must carefully account but which the 3ω technique is insensitive in the frequency domain. Therefore, these effects can be treated as an offset in 3ω analysis [16].

2 Suspended Test Structures

The SUMMiT V™ process [22] involves four structural *n*-type (phosphorous-doped) polysilicon layers with a fifth layer as a ground plane. The polysilicon layers are separated by sacrificial oxide layers that are etched away during the final release step. The two topmost layers, Poly3 and Poly4, are nominally 2.25 μm in thickness, while the bottom two, Poly1 and Poly2, are nominally 1.0 μm and 1.25 μm in thickness, respectively. The ground plane, Poly0, is 300 nm in thickness and lies above an 800 nm layer of silicon nitride and a 630 nm layer of silicon dioxide. The sacrificial oxide layers between the structural layers are each roughly 2.0 μm thick.

The thermal conductivity test structures are fabricated from the Poly4 layer and are nominally 2.25 μm thick. Test structures were designed with a width of 10 μm and four lengths: 200 μm, 300 μm, 400 μm, and 500 μm. The fixed-fixed bridge ends at bond pads, which are layered structures that mechanically anchor the beam to the substrate and provide a location for wire bonding to the package. The wires are bonded to a 700 nm layer of Al that is deposited on top of the bond pad. Figure 1 is an image of a 10 μm wide and 200 μm long suspended bridge test structure used in this study with the bond pads and bond wires visible.

3 3ω Experimental Considerations

As previously mentioned, the thermal conductivity of the Poly4 SUMMiT V™ bridge structures were measured with both steady state and 3ω techniques. Details of the steady state experimental setup, analysis, assumptions, and possible errors are described in

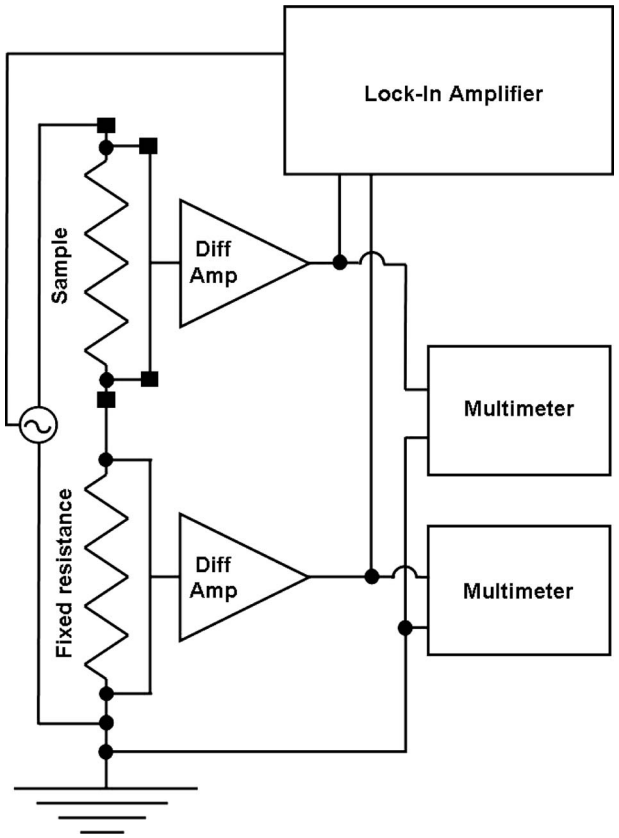

Fig. 2 Schematic representing circuit and data acquisition equipment in the 3ω measurements. The sample is the polysilicon microbridge structure, and the fixed resistance varied depending on the sample. The value of the fixed resistance was chosen to be slightly higher than the maximum resistance across the sample [14]. During testing, this value was set to be slightly higher than the room temperature resistance of the sample.

Refs. [11,24]. A description of the 3ω setup used for measurements on the Poly4 SUMMiT V™ bridge structure follows. Figure 2 shows a schematic of the electrical circuit with the data acquisition components of the experimental setup. This is essentially the same setup as Cahill's original experiment [14,15] only the use of a SR830 digital signal processing (DSP) lock-in amplifier with higher harmonic detection removes the need for a frequency tripling circuit. This lock-in greatly simplifies the circuit since it was used for the input current, reference signal, and measurement of the third harmonic (3ω) voltage. The ac sinusoidal input current, which was supplied by the lock-in amplifier, was passed through the sample and resistor of fixed resistance. Passing the resulting voltage drops through AD534 differential amplifiers reduces unwanted noise by producing a signal equal to the voltage drop across the sample and fixed resistor, respectively. The resulting signals were then differenced by the lock-in amplifier. Differencing the two resulting voltages across the sample and fixed resistor removed the majority of unwanted noise. The differenced voltage signal contains both ω and 3ω components. The lock-in amplifier was used to detect the small resulting 3ω component by comparing the differenced voltage signal with the input current (supplied by the lock-in amplifier).

The temperature dependent data were obtained while slowly heating and cooling the test structures in a liquid nitrogen cooled Henriksen cryostat that was pumped down to less than 1 mTorr. Only the sample is in the temperature controlled vacuum; the fixed resistor is wired in the circuit in ambient so that it experiences minimal temperature fluctuations. The voltage dissipated

across the sample and fixed resistor was determined with Agilent 34401A multimeters, and then the resistance across the test section was determined at each temperature. Since the majority of the resistance between the voltage probes on the bond pads lies in the bridge structure, the 3ω data were analyzed with the relationship between 3ω voltage and thermal conductivity derived by Lu et al. [21] for one-dimensional conduction along rodlike structures, given by

$$V_{3\omega} \approx \frac{4V^3L}{\pi^4 kAR^2\sqrt{1+(2\omega\gamma)^2}}\frac{dR}{dT} \tag{1}$$

where V and $V_{3\omega}$ are the voltage dissipated across the bridge structure and the third harmonic of the voltage detected across the bridge structure, respectively; L is the length of the bridge structure (the additional length from the bridge-bond pad connection was neglected since the lateral resistance in the bond pad is considered negligible compared with the resistance along the bridge structure); k is the thermal conductivity of the bridge structure; A is the cross-sectional area of the bridge structure; R is the electrical resistance measured across the bridge structure; ω is the angular frequency of the ac supplied to the circuit; and γ is the characteristic thermal time constant for the axial thermal process, which for this one-dimensional thermal process is defined as $\gamma = L^2C/\pi^2 k$ [21], where C is the heat capacity of the structure, and dR/dT is the change in the electrical resistance over the temperature range for the measurements. The electrical resistance as a function of temperature was determined from the voltage drop across the test section (ts) and fixed resistor (fr) and the resistance of the fixed resistor by $R_{ts}=R_{fr}V_{ts}/V_{fr}$. The measured dR/dT of the 200 μm, 300 μm, 400 μm, and 500 μm long bridges were 0.226 Ω/K, 0.328 Ω/K, 0.443 Ω/K, and 0.554 Ω/K, respectively. The temperature dependent resistance values measured using the steady state experimental technique were similar: 0.224 Ω/K, 0.334 Ω/K, 0.454 Ω/K, and 0.553 Ω/K, respectively. The electrical resistance of the test section exhibited a linear trend with temperature over the entire temperature range of interest; therefore dR/dT was constant. 3ω data were taken over a wide range of frequencies. At relatively low frequencies, where the thermal wavelength is much larger than the length of the structure, $\omega\gamma$ approaches zero and the resulting 3ω voltage is frequency independent. In this limit, Eq. (1) becomes

$$V_{3\omega} \approx \frac{4V^3L}{\pi^4 kAR^2}\frac{dR}{dT} \tag{2}$$

and the thermal conductivity can be easily determined from the in-phase portion of $V_{3\omega}$.

Figure 3 shows the $V_{3\omega}$ response on a 200 μm microbridge test structure at 294 K along with the best fit of Eq. (1) using k and γ as fitting parameters. The thermal conductivity is determined from the low frequency data, where the 3ω response is frequency independent. The time constant γ then determines the curvature of the 3ω response at higher frequencies. The best fit thermal conductivity of this structure is 66 W m^{-1} K^{-1}. The thermal time constant γ of this structure is 1.199 ms, as shown from the best fit of Eq. 1 in Fig. 3. Equation (1), solved with two other time constants of γ=0 s and γ=10 ms, is also shown in this figure.

During testing, the frequency range was swept from 5 rad s^{-1} to 10,000 rad s^{-1} during data collection at room temperature and low temperature (85 K). This identified the region of frequency independent $V_{3\omega}$ and also determined the maximum and minimum time constants of the structure over the temperature range. Data were taken at temperatures ranging from 85 K to 294 K. The temperature of the cryostat was ramped at 1.0 K/min and only a few selected frequencies in the frequency independent $V_{3\omega}$ range (low frequencies) were applied to the circuit so that the frequency range was swept approximately three times before the chamber changed 1 K.

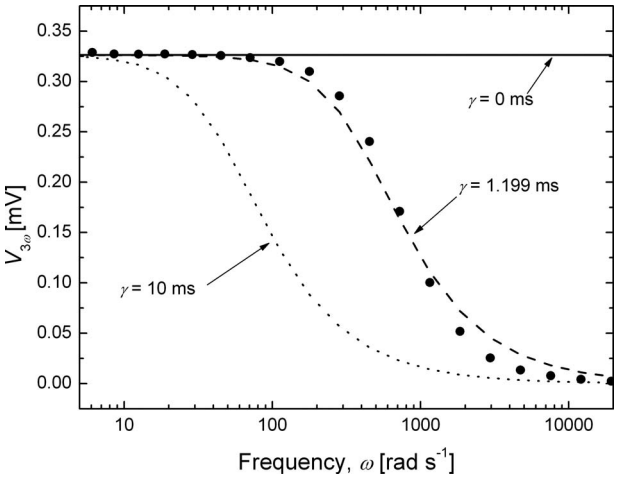

Fig. 3 Sensitivity of Eq. (1) to the thermal time constant γ. A best fit thermal conductivity k is 66 W m^{-1} K^{-1}. The thermal conductivity of the test structures is easily determined by identifying the region of frequency independent $V_{3\omega}$ and fitting Eq. (2) to the data.

4 Results

Figure 4 shows Eq. (1) fit to 3ω data on the different length bridge structures taken at 85 K and 294 K. The thermal conductivity k and time constant γ, determined from Eq. (1), are also shown in this figure. The data and Eq. (1) fit are normalized for clarity since the value of $V_{3\omega}$ is different for each bridge structure. As the bridge length decreases, the thermal time constant also decreases. This is expected since a shorter bridge structure will take less time to equilibrate. In addition, the time constant in each structure decreases as the temperature decreases. This causes the region of frequency independent $V_{3\omega}$ response to span a longer frequency range. Figure 5 summarizes the thermal time constant results from the data shown in Fig. 4. The time constant, which increases at higher temperatures, is related to the phonon mean free path and equilibration time. At lower temperatures, the phonon mean free path is longer than at higher temperatures, and the bridge structures take less time to equilibrate. The longer bridge structures also take more time to equilibrate than the shorter bridge structures since the longer bridge structures create more scattering events along the length of the bridge, which in turn leads to longer equilibration time.

Figure 6 compares the thermal conductivity of the four bridge structures taken with the 3ω technique to the thermal conductivity determined with the steady state method. The thermal conductivity 3ω data are reported in increments of 1.0 K. As previously motioned, there were approximately three frequency sweeps taken before the sample changed 1 K, so each data point in the 3ω represents the statistical average of three measurements. The standard deviation among the three measurements at each temperature increment is less than 2% for all temperatures; the sizes of the data points are greater than the uncertainty among the three measurements at each temperature.

Notice there is a length dependency in the thermal conductivity measurements, which could arise from the contact resistance at the bridge/bond pad junction [24]. This dependency is far less apparent in the 3ω data taken at lower temperatures, but at higher temperatures, the same dependency exists between the 3ω and the steady state measurements. Some of the length dependency error has been considered in the steady state analysis by examining bond pad heating [24]. Some length dependency error could also result from the geometry of the test structure; for example, the electrical connections are placed on the bond pads and not on the suspended test structure. This could add to the measured electrical

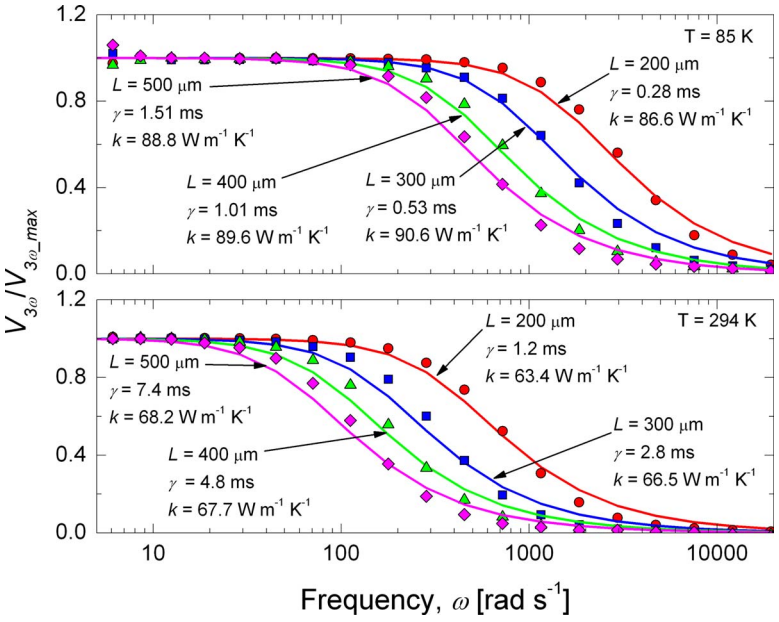

Fig. 4 3ω voltage on the different length bridge structures with the Eq. (1) fit to the data with best fit *k* and γ. The data and best fit are normalized for clarity. The frequency independent region of the 3ω voltage responses increases with a decrease in temperature.

resistance and subsequent thermal conductivity measurements. In addition, the locations of the electrical connections on the bond pads are not exact for each sample, which would also add to the error among the samples. The measured thermal conductivities of the bridge structures should not be length dependent (at these bridge lengths of several hundred microns), and the length dependencies are associated with measurement and instrumentation errors. The 3ω measurements appear to be less sensitive to these errors.

Figure 7 shows the 3ω measured thermal conductivity compared with the steady state data over the temperature range from 85 K to 294 K. The steady state thermal conductivity data on the bridge structures are larger than the thermal conductivity determined with the 3ω technique, especially at low temperature. The temperature trends and values of the 3ω data show much better agreement with literature values for polysilicon [3,5,8–10] than the steady state measurements.

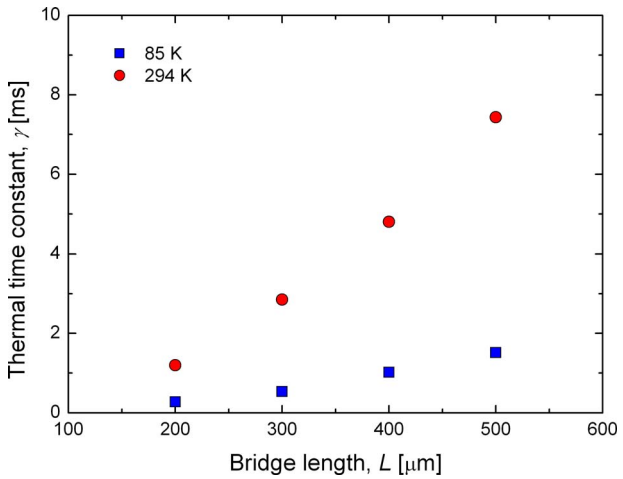

Fig. 5 Thermal time constant γ as a function of bridge length *L* determined at two different temperatures

In comparison of the 3ω polysilicon thermal conductivity to other reported values, potential for radiative heat losses must be considered; convective heat losses are considered negligible for microstructures under high vacuum [7,12,13,21]. These 3ω tests were conducted in a vacuum chamber with a maximum pressure of 1 mTorr and recent experimental and theoretical results have shown that convective losses can be neglected at pressures below 500 mTorr on samples with identical geometries subject to similar testing conditions [25].

Radiative heat loss per unit time per unit length W from a bridge with a rectangular cross section of area $A=d\times w$, where d is the thickness and w is the width of the bridge, to the environment of temperature T_0 is given by

$$W(x,t) = 2\varepsilon\sigma(d+w)[T^4(x,t) - T_0^4] \tag{3}$$

where ε is the emissivity of the polysilicon surface, σ is the Stefan–Boltzmann constant (5.67×10^{-8} W m^{-2} K^{-4}), x is the position along the polysilicon film, and t is the time. Defining an impulse function $\Delta(x,t)$, which represents the integral of the responses of the bridge to the instant "force" of current at each time interval [21], Eq. (3) can be approximated as

$$W \approx 8\varepsilon\sigma(d+w)T_0^3\Delta(x,t) \tag{4}$$

Following a similar analysis to the cylindrical rod radiation loss calculation by Lu et al. [21], the radiation heat loss coefficient g for a bridge with a rectangular cross section is given by

$$g = \frac{8\varepsilon\sigma(d+w)T_0^3}{Cdw} \tag{5}$$

Radiation heat loss can be neglected if $g\gamma \ll 1$. Taking the worst case scenario from the measured time constants in Fig. 5 for a 500 μm bridge at 294 K with γ=7.5 ms and assuming an emissivity of unity and bulk Si heat capacity of $C=1.66\times10^6$ J m^{-3} K^{-1} [26] yields a criterion value of 2.8×10^{-2}, which is low enough to neglect radiation losses. However, to avoid inaccuracies from using bulk values for heat capacity, the mathematical definition of γ can be used with Eq. (5) to yield a crite-

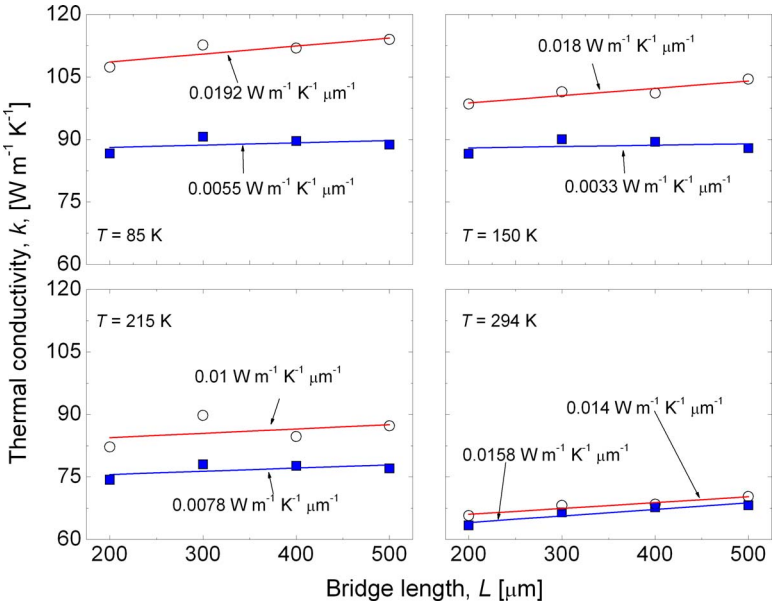

Fig. 6 Thermal conductivity measured with the 3ω (filled squares) and steady state (empty circles) [11] techniques as a function of bridge length at four different temperatures. The dependency of the data on bridge length is shown by the slope of the best fit line to the data. The bridge length dependency is essentially nonexistent in the lower temperature 3ω data, which is apparent by comparing the thermal conductivity trends with bridge length represented by the slopes of the best fit line to the data that are listed in the figures.

rion value based on the thermal conductivity measurements given by

$$\frac{8\varepsilon\sigma(d+w)T_0^3L^2}{\pi^2 dwk} \ll 1 \tag{6}$$

Taking the 500 μm bridge at 294 K with a measured k of 67 W m^{-1} K^{-1} yields a criterion value of 2.35×10^{-3}, using Eq. (6), which is certainly low enough to neglect radiation heat loss [7].

As previously mentioned, electrical and thermal resistances in the bond pads not associated with the test structure for which the 3ω measurements are insensitive in the frequency domain can be treated as an offset to the measured thermal conductivity [16]. Electrical resistance and bond pad offsets were neglected in the

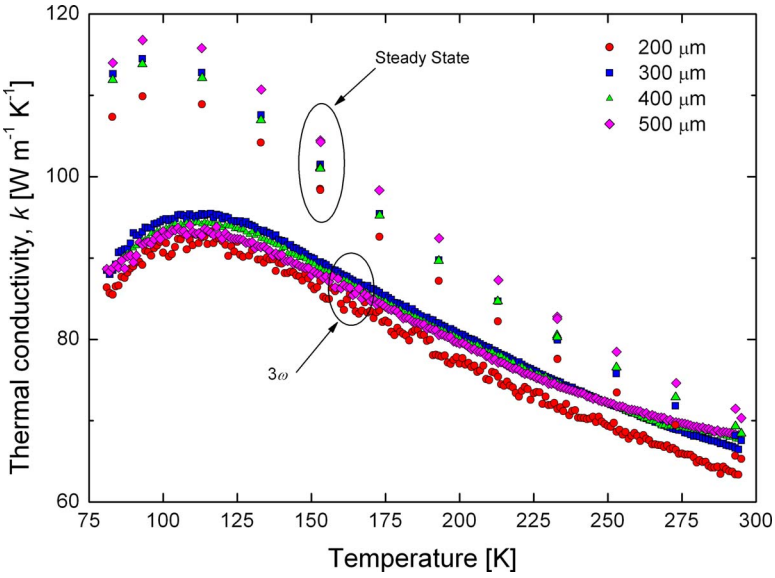

Fig. 7 Temperature dependent thermal conductivity data on the polysilicon bridge test structures. The 3ω and steady state measurements are both presented for comparison. The differences between the two sets of data determined from the different measurement techniques can be explained by the effects of bond pad heating and thermal boundary resistance between the Al wire bonded film and the bond pad.

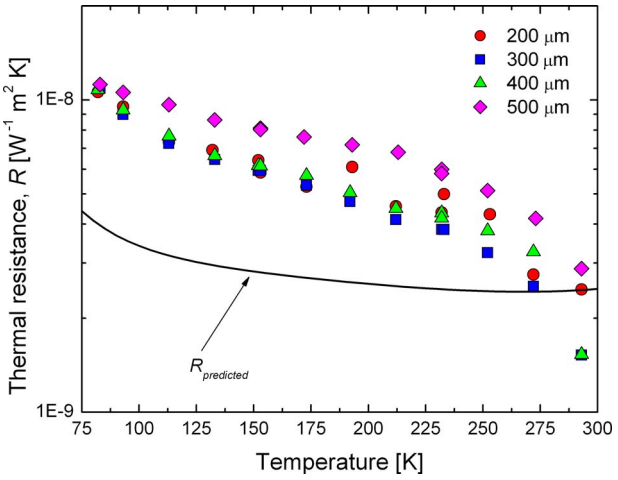

Fig. 8 Additional thermal resistances determined from the two data sets in Fig. 7 and Eq. (7) compared with the predicted thermal resistance $R_{predicted}$ of the 700 nm Al bond pad the Al/Si interface

analysis of the steady state data [11]. The lumped thermal resistance of the Al film to which the wires are bonded and the thermal boundary resistance [27] between the Al and the P4 polysilicon layer on the bond pad could play a significant role in thermal conductivity measurements, which may explain the difference between the 3ω and steady state measurements at the lower temperatures. To compare the steady state and 3ω measurements, these considerations are addressed in more detail by lumping these resistances into an interface resistance formulation. The thermal resistance not in the bridge test structure R is estimated by [16]

$$R = d\left(\frac{1}{k_{3\omega}} - \frac{1}{k_{ss}}\right) \tag{7}$$

where $k_{3\omega}$ is the thermal conductivity measured with the 3ω technique, k_{ss} is the thermal conductivity measured with the steady state technique, and d is the thickness of the P4 polysilicon layer. Since the 3ω technique is insensitive to the Al pad and interface resistances, the thermal conductivity determined with the 3ω technique represents the thermal conductivity of the polysilicon microbridge. The steady state measurements represent the thermal conductivity measured from voltage connection to voltage connection, which includes heat flow through the bond pads and is sensitive to the thermal resistances of the two Al bond pads and the thermal boundary resistances between the Al and the P4 structures. Using Eq. (7) the additional thermal resistance R is calculated from the difference between the two data sets shown in Fig. 7. Equation (7) calculations are shown in Fig. 8 along with calculations for an interface resistance assuming two parallel thermal resistors of a 700 nm Al film and an Al/Si interface. Using a lumped thermal resistance for the Al bond bad, and assuming a thermal conductivity of bulk Al, the Al film's thermal resistance is given by $R_{Al}=d_{Al}/k_{Al}$, where the temperature dependent thermal conductivity is taken from experimental data [28]. Using a bulk Al thermal conductivity for the 700 nm bond pad is valid since the electron mean free path in Al is approximately 50 nm [29]. The thermal resistance of an Al/Si interface is estimated from the diffuse mismatch model (DMM) [27]. The total resistance is then estimated as $R_{predicted}=(R_{Al}+R_{DMM})/2$.

To apply the DMM in its simplest form, the following assumptions are made [30]: (1) phonons are elastically scattered, (2) phonon scattering is completely diffused, and (3) the materials on either side of the interface are treated as Debye solids giving constant longitudinal and transverse acoustic velocities throughout the Brillouin zone. Using the DMM, the thermal boundary resistance R_{DMM} from side 1 (Al) to side 2 (Si) can be calculated by

$$\frac{1}{R_{DMM}} = \frac{1}{4}\sum_j u_{1,j}\int_0^{\nu_{1,j}^c} \alpha_1 h\nu D_{1,j}(\nu)\frac{\partial n(\nu,T)}{\partial T}d\nu \tag{8}$$

where the subscripts 1 and j refer to the side and the mode (with one longitudinal mode and two transverse modes, so Eq. (8) is summed over the three modes), respectively, ν is the phonon frequency, u is the phonon velocity, $\nu_{1,j}^c$ refers to the cutoff frequency of mode j on side 1, α is the phonon transmission coefficient, h is Planck's constant, D is the spectral phonon density of states per unit volume, and n is the Bose–Einstein distribution function. With assumption (3) discussed above, the Debye density of states per unit frequency per unit volume is given by

$$D_{1,j}(\nu) = \frac{2\nu^2}{u_{1,j}^3} \tag{9}$$

which leads to the cutoff frequency of mode j on side 1 being defined as [30]

$$\nu_{1,j}^c = u_{1,j}\left(\frac{3N_1}{4\pi}\right)^{1/3} \tag{10}$$

where N_1 is the total number of oscillators per unit volume of side 1. In cubic structures, such as Al, $N=\rho N_A/M$, where ρ is the mass density, N_A is Avogadro's number, and M is the atomic weight. The Bose–Einstein distribution function is defined as

$$n(\nu,T) = \frac{1}{\exp\left[\dfrac{h\nu}{k_B T}\right] - 1} \tag{11}$$

where k_B is Boltzmann's constant, and the phonon transmission coefficient from side 1 (Al) to side 2 (Si) under the three assumptions discussed above is defined as [27]

$$\alpha_1 = \frac{\sum_j u_{2,j}^{-2}}{\sum_j u_{1,j}^{-2} + \sum_j u_{2,j}^{-2}} \tag{12}$$

With Eqs. (8)–(12), R_{DMM} is calculated for an Al/Si interface as a function of temperature, as shown in Fig. 8. For these calculations, taking Al as side 1 and Si as side 2, the following thermophysical parameters were used [27]: $u_{1,L}=6240$ m s^{-1}, $u_{1,T}=3040$ m s^{-1}, $u_{2,L}=8970$ m s^{-1}, $u_{2,T}=5332$ m s^{-1}, $\rho_1=2700$ kg m^{-3}, and $M_1=0.027$ kg mol^{-1}.

The thermal boundary resistance determined from the comparison of the steady state and 3ω data (via Eq. (7)) shows agreement within an order of magnitude of the DMM calculations. This could be due to several aspects of the microbridge test samples not taken into account in DMM calculations such as temperature gradients in the bond pad due to Joule heating, changes in geometry at the bridge/bond pad junction, and additional carriers in the polysilicon due to the phosphorous dopants. The low temperature trends in the DMM are driven by phonon quantum state filling in accordance with the Bose–Einstein statistical distribution. The matching R trends in the Fig. 8 data at low temperatures suggest that the deviation in the temperature trends between the steady state and 3ω data are due to phonon-phonon scattering in thermal boundary conductance. At higher temperatures R rapidly decreases in the Eq. (7) calculations but approaches a constant value in the DMM calculations. The trend in the experimentally determined R could be due to electron-electron conductance at the interface, which contributes a linear temperature trend to thermal boundary resistance [31].

Although the discrepancies between the steady state and 3ω experimental measurements are explained, in part, by the thermal boundary resistance between the Al contact and the bond pad,

there are other experimental aspects that could be contributing to the different measurements. For example, the silicon microbridges are polycrystalline, and the differing sensitivities of the 3ω and steady state techniques to grain boundaries are relatively unknown. Also, the geometric change from the bond pad to the microbridge could lead to different types of responses. In addition, the steady state data show a length dependency, which could be due to analysis techniques on the raw data involving bond pad heating [24]. A similar analysis may be appropriate for the 3ω data.

5 Conclusions

Thermal conductivity measurements were made on polysilicon microbridges that were 10 μm wide and ranged from 200 μm to 500 μm long with the 3ω technique and compared with measurements made on the same structures with a steady state resistance technique. The measurements with the 3ω technique exhibit less of a dependence on length than the steady state measurements and agree much better with previously reported values of thermal conductivity of polysilicon microbridges. An explanation for the differences between the conductivities measured with the two different techniques is the thermal resistances of the Al and polysilicon layers in the bond pad.

Acknowledgment

The authors would like to thank Pam Norris at University of Virginia for her insight and arranging this collaboration, and Rebecca Clemens, Jaron Kuppers, Allen Gorby, and David Epp at Sandia for assistance with various aspects of the 3ω experimental setup. P.E.H. greatly appreciates financial support from the NSF graduate research fellowship program and a Sandia National Laboratories summer internship. Sandia is a multiprogram laboratory operated by Sandia Corporation, a Lockheed-Martin Co., for the United States Department of Energy's National Nuclear Security Administration under Contract No. DE-AC04-94AL85000.

Nomenclature

A = cross-sectional area, m^2
C = heat capacity, J m^{-3} K^{-1}
D = spectral phonon density of states, s m^{-3}
d = bridge thickness, m
g = radiation heat loss coefficient, s^{-1}
h = Planck's constant, J s
k = thermal conductivity, W m^{-1} K^{-1}
k_B = Boltzmann's constant, J K^{-1}
L = bridge length, m
M = atomic weight, kg mol^{-1}
N = oscillators per unit volume, m^{-3}
N_A = Avogrado's number, mol^{-1}
n = Bose–Einstein distribution function
R = electrical resistance, Ω
R_{BD} = thermal boundary resistance, W^{-1} m^2 K
T = temperature, K
t = time, s
u = phonon velocity, m s^{-1}
V = voltage, V
W = power loss per unit length, W m^{-1}
w = bridge width, m
x = positions, m

Greek Symbols

α = phonon transmission coefficient
Δ = impulse function, K
γ = thermal time constant, s
ε = emissivity
ν = phonon frequency, s^{-1}
ρ = mass density, kg m^{-3}
σ = Stefan–Boltzmann constant, W m^{-2} K^{-4}
ω = angular frequency, rad s^{-1}

Subscripts

1 = side 1
3ω = third harmonic
cl = convection loss
DMM = calculated with the DMM
i = intrinsic
j = phonon mode (longitudinal or transverse)
L = longitudinal mode
m = measured
T = transverse mode

Superscripts

c = cutoff

References

[1] Smith, A. N., and Calame, J. P., 2004, "Impact of Thin Film Thermophysical Properties on Thermal Management of Wide Bandgap Solid-State Transistors," Int. J. Thermophys., **25**, pp. 409–422.
[2] Cahill, D. G., Ford, W. K., Goodson, K. E., Mahan, G. D., Majumdar, A., Maris, H. J., Merlin, R., and Phillpot, S. R., 2003, "Nanoscale Thermal Transport," J. Appl. Phys., **93**, pp. 793–818.
[3] Mcconnell, A. D., Uma, S., and Goodson, K. E., 2001, "Thermal Conductivity of Doped Polysilicon Layers," J. Microelectromech. Syst., **10**, pp. 360–369.
[4] Cahill, D. G., Goodson, K. E., and Majumdar, A., 2002, "Thermometry and Thermal Transport in Micro/Nanoscale Solid-State Devices and Structures," ASME J. Heat Transfer, **124**, pp. 223–241.
[5] Uma, S., Mcconnell, A. D., Ashegi, M., Kurabayashi, K., and Goodson, K. E., 2001, "Temperature-Dependent Thermal Conductivity of Undoped Polycrystalline Silicon Layers," Int. J. Thermophys., **22**, pp. 605–616.
[6] Asheghi, M., Kurabayashi, K., Kasnavi, R., and Goodson, K. E., 2002, "Thermal Conduction in Doped Single-Crystal Silicon Films," J. Appl. Phys., **91**, pp. 5079–5088.
[7] Park, K., Marchenkov, A., Zhang, Z. M., and King, W. P., 2007, "Low Temperature Characterization of Heated Microcantilevers," J. Appl. Phys., **101**, p. 094504.
[8] Paul, O. M., Korvink, J., and Baltes, H., 1994, "Determination of the Thermal Conductivity of CMOS IC Polysilicon," Sens. Actuators, A, **41**, pp. 161–164.
[9] Von Arx, M., Paul, O., and Baltes, H., 2000, "Process-Dependent Thin-Film Thermal Conductivities for Thermal CMOS MEMS," J. Microelectromech. Syst., **9**, pp. 136–145.
[10] Volklein, F., and Baltes, H., 1992, "A Microstructure for Measurement of Thermal Conductivity of Polysilicon Thin Films," J. Microelectromech. Syst., **1**, pp. 193–196.
[11] Phinney, L. M., Kuppers, J. D., and Clemens, R. C., 2006, "Thermal Conductivity of SUMMiT™ V Polycrystalline Silicon," Sandia National Laboratories, Report No. SAND2006-7122.
[12] Tai, Y. C., Mastrangelo, C. H., and Muller, R. S., 1988, "Thermal Conductivity of Heavily Doped Low-Pressure Chemical Vapor Deposited Polycrystalline Silicon Films," J. Appl. Phys., **63**, pp. 1442–1447.
[13] Tai, Y. C., Mastrangelo, C. H., and Muller, R. S., 1989, "Erratum: 'Thermal Conductivity of Heavily Doped Low-Pressure Chemical Vapor Deposited Polycrystalline Silicon Films' [J. Appl. Phys. 63, 1442 (1988)]," J. Appl. Phys., **66**, pp. 3420.
[14] Cahill, D. G., 1990, "Thermal Conductivity Measurement From 30 to 750 K: The 3ω Method," Rev. Sci. Instrum., **61**, pp. 802–808.
[15] Cahill, D. G., 2002, "Erratum: 'Thermal Conductivity Measurement From 30 to 750 K: The 3ω Method' [Rev. Sci. Instrum. 61, 802 (1990)]," Rev. Sci. Instrum., **73**, p. 3701.
[16] Lee, S.-M., and Cahill, D. G., 1997, "Heat Transport in Thin Dielectric Films," J. Appl. Phys., **81**, pp. 2590–2595.
[17] Lee, S.-M., Cahill, D. G., and Venkatasubramanian, R., 1997, "Thermal Conductivity of Si-Ge Superlattices," Appl. Phys. Lett., **70**, pp. 2957–2959.
[18] Borca-Tasciuc, T., Kumar, A. R., and Chen, G., 2001, "Data Reduction in 3ω Method for Thin-Film Thermal Conductivity Determination," Rev. Sci. Instrum., **72**, pp. 2139–2147.
[19] Olson, B. W., Graham, S., and Chen, K., 2005, "A Practical Extension of the 3ω Method to Multilayer Structures," Rev. Sci. Instrum., **76**, p. 053901.
[20] Dames, C., and Chen, G., 2005, "1ω, 2ω, and 3ω Methods for Measurements of Thermal Properties," Rev. Sci. Instrum., **76**, p. 124902.
[21] Lu, L., Yi, W., and Zhang, D. L., 2001, "3ω Method for Specific Heat and Thermal Conductivity Measurements," Rev. Sci. Instrum., **72**, pp. 2996–3003.
[22] "SUMMiT V™: Five Level Surface Micromachining Technology and Design Manual," 2007, MEMS Technology Department, Sandia National Laboratories, Report No. SAND2007-D0446.
[23] Sniegowski, J. J., and De Boer, M. P., 2000, "IC-Compatible Polysilicon Surface Micromachining," Annu. Rev. Mater. Sci., **30**, pp. 299–333.
[24] Phinney, L. M., Piekos, E. S., and Kuppers, J. D., 2007, "Bond Pad Effects on Steady State Thermal Conductivity Measurement Using Suspended Micromachined Test Structures," *Proceedings of the 2007 ASME International Me-*

chanical Engineering Congress and Exposition, Seattle, WA, Paper No. 41349.
[25] Torczynski, J. R., Gallis, M. A., Piekos, E. S., Phinney, L. M., Serrano, J. R., and Gorby, A. D., 2008, "Validation of Thermal Models for a Prototypical MEMS Thermal Actuator," Sandia National Laboratories, Report No. SAND2008-D5749.
[26] Incropera, F., and Dewitt, D. P., 1996, *Fundamentals of Heat and Mass Transfer*, Wiley, New York.
[27] Swartz, E. T., and Pohl, R. O., 1989, "Thermal Boundary Resistance," Rev. Mod. Phys., **61**, pp. 605–668.
[28] Ho, C. Y., Powell, R. W., and Liley, P. E., 1972, "Thermal Conductivity of the Elements," J. Phys. Chem. Ref. Data, **1**, pp. 279–422.
[29] Hohlfeld, J., Wellershoff, S.-S., Gudde, J., Conrad, U., Jahnke, V., and Matthias, E., 2000, "Electron and Lattice Dynamics Following Optical Excitation of Metals," Chem. Phys., **251**, pp. 237–258.
[30] Cahill, D. G., Bullen, A., and Lee, S.-M., 2000, "Interface Thermal Conductance and the Thermal Conductivity of Multilayer Thin Films," High Temp. - High Press., **32**, pp. 135–142.
[31] Gundrum, B. C., Cahill, D. G., and Averback, R. S., 2005, "Thermal Conductance of Metal-Metal Interfaces," Phys. Rev. B, **72**, p. 245426.